Materials Chemistry and Physics 256 (2020) 123627

Contents lists available at ScienceDirect

Materials Chemistry and Physics

journal homepage: www.elsevier.com/locate/matchemphys

Materials science communication

# Enhanced corrosion resistance and surface bioactivity of AZ31B Mg alloy by high pressure cold sprayed monolayer Ti and bilayer Ta/Ti coatings in simulated body fluid

M. Daroonparvar [a,b,*], M.U. Farooq Khan [c], Y. Saadeh [c], C.M. Kay [a], R.K. Gupta [c,**], A.K. Kasar [d], P. Kumar [b], M. Misra [b], Pradeep L. Menezes [d], H.R. Bakhsheshi-Rad [e]

[a] Research and Development Department, ASB Industries. Inc, Barberton, OH, 44203, USA
[b] Department of Chemical and Materials Engineering, University of Nevada, Reno, NV, 89501, USA
[c] Department of Chemical, Biomolecular, and Corrosion Engineering, The University of Akron, Akron, OH, 44325, USA
[d] Department of Mechanical Engineering, University of Nevada, Reno, NV, 89501, USA
[e] Advanced Materials Research Center, Department of Materials Engineering, Najafabad Branch, Islamic Azad University, Najafabad, Iran

## HIGHLIGHTS

- Ta/Ti coating considerably lowered the wear rate of AZ31B Mg alloy.
- Active dissolution of Mg alloy was substantially lowered by Ti coating.
- A dense layer of Ta on Ti coating greatly enhanced corrosion resistance of Ti/Mg.
- $R_{ct}$ and $|Z|_{f=0.01Hz}$ values for Ta/Ti/Mg remained slightly stable during immersion.
- Island-like surface of coatings improved the bioactivity of AZ31BMg alloy.

## ARTICLE INFO

*Keywords:*
Mg alloy
Cold spray
Protective coatings
Corrosion resistance
Bioactivity

## ABSTRACT

Ti and Ta/Ti coatings were successfully applied on AZ31B Mg alloy using high pressure cold spray process. These coatings (particularly Ta/Ti coating) with high hardness lowered the wear rate of AZ31BMg alloy. In-vitro bioactivity test, infinite focus 3D measurement and EDS results revealed that the calcium-phosphate (Ca–P) compounds nucleation and growth capabilities on both the coatings surface are higher than AZ31B Mg alloy surface due to the highly passivating nature and rough surface (island-like) of the high pressure cold sprayed Ti and Ta/Ti coatings, which are further conducive to the biological fixation. Electrochemical corrosion and immersion tests disclosed that a dense layer of Ta on Ti coating was able to enhance the corrosion resistance of Ti/AZ31B Mg system in the Hank's balanced salt solution. $R_{ct}$ (charge transfer resistance) and $|Z|_{f=0.01Hz}$ values for Ta/Ti coated Mg alloy have remained slightly stable. This imparted that the rate of electrochemical processes at the electrode/electrolyte interface could remain very slow in the course of immersion time. Likewise, the OCP (open circuit potential) values of Ta/Ti coating remained constant during long term electrochemical corrosion test. This behavior could originate from fairly dense structure of the high pressure cold sprayed Ta layer which considerably impeded the penetration of corrosive solution into the coating interiors. Ta/Ti coating presented the most positive potential, highest $R_{ct}$, and highest$|Z|_{f=0.01Hz}$ values, suggesting that it is the most thermodynamically stable/least to be corroded in Hank's balanced salt solution over time. In general, cold sprayed Ta/Ti coating might open a new way to broaden the utilization of Mg alloys in the field of biomaterials.

* Corresponding author. Department of Chemical and Materials Engineering, University of Nevada, Reno, NV, 89501, USA
** Corresponding author.
*E-mail addresses:* mr.daroonparvar@yahoo.com (M. Daroonparvar), rgupt@uakron.edu (R.K. Gupta).

https://doi.org/10.1016/j.matchemphys.2020.123627
Received 22 February 2020; Received in revised form 20 July 2020; Accepted 28 July 2020
Available online 18 August 2020

## 1. Introduction

Mg and its alloys have amazing advantages over the titanium alloy as most popular implant material [1], such as low density which is very close to that of human bone (1.75 g/cm$^3$), higher specific strength and low elastic modulus [2–5]. However, high degradation rate of Mg (because of low standard reduction potential (−2.37 $V_{SHE}$)) is accompanied by the localized hydrogen evolution in $Cl^-$ containing solutions [2–9]. Formation of more loose degradation products on the alloy surface and continuation of metal matrix dissolution occur as the degradation phenomenon continues. This led to the partial separation of the metal matrix during corrosion. This also resulted in the exposure of fresh metal matrix in the corrosive electrolyte and new round of severe degradation [10]. Hence, these phenomena considerably restricted the biomedical applications of the Mg alloys [2,3,4,6,7,8,and10].

Over the years, several techniques [9,11] have been developed to modify the Mg surface for lowering the corrosion and wear rates [4,7,9, 12–15]. With respect to the low standard reduction potential (SRP) mismatch between Ti and Mg, E. Zhang et al. [2] and D. Zhang et al. [16] applied Ti (having high passivation propensity) coating on Mg using ion plating and magnetron sputtering methods, respectively. Corrosion current density ($i_{corr}$) of Mg declined with Ti coatings by only one order of magnitude. Moreover, porous (4.25–7.25%) warm sprayed Ti coatings formed a galvanic cell with the AZ91E Mg alloy substrate [17]. This galvanic coupling led to the formation and severe accumulation of corrosion products at the Ti coating/Mg alloy interface and thus premature rupture of the coatings after only 1 day of immersion in chloride-containing solution [17].

Among these methods, cold spray (CS) process (as relatively new coating technology) uses kinetic energy to produce the coating layer rather than a combination of thermal and kinetic energies such as HVOF (high velocity oxygen fuel) spray process. Fine powder particles (5–50 μm) are propelled toward the substrate surface with supersonic velocity (300–1200 m/s). Upon impact, the particles undergo adiabatic heating and plastically deform at very high shear rates, which leads to flattening and strong bonding them to the underlying surface (material jets) [18, 19]. Moreover, cold spray process could impede the microstructural damage of the heat-vulnerable substrates such as Mg alloys which is often observed in the alternative thermal and plasma spray methods [20–23]. Furthermore, cold sprayed coatings considerably increased the corrosion resistance of AZ31 and AZ91 Mg alloys (in chloride containing solutions) compared to the other coatings produced by techniques such as anodizing, E-plating and chemical conversion coating [24].

In recent years, cold sprayed Ti coatings have been extensively studied and developed [25–28]. This coating slightly lowered the corrosion rate of Mg alloys [26]. Nevertheless, post-spray treatments should be performed on as-cold sprayed Ti coatings (with H.C.P crystal structure and lower slip systems) to enhance their denseness [25,26,28]. Recently, Ta having a low SRP mismatch with Ti, excellent passivation tendency, better bioactivity, and biocompatibility [29,30] was applied on Ti substrates to enhance their wear and corrosion resistances [30,31]. Motivated by the above-mentioned facts, we developed Ta/Ti coating on AZ31BMg alloys using high pressure cold spray process. In this work, it is anticipated that a compact layer of Ta (with B.C.C crystal structure, noticeable bioactivity and lower wear rate) on the cold sprayed Ti coating could considerably lower the corrosion rate of Ti/AZ31B Mg system in the SBF solution. Therefore, corrosion performance of cold sprayed Ti and Ta/Ti coatings have been studied using electrochemical methods and surface characterization.

## 2. Materials and experiments

Commercially pure (CP)–Ti grade 1 and high purity spherical Ta powders were used as feedstock powder materials in this research. The substrates were cut from commercially available AZ31B Mg alloy plate (chemical composition is provided in the Supporting Information (S1)). Prior to the cold spray process, the substrate surface was blasted with 46 grit aluminum oxide media (detailed procedure in Supporting Information (S2)). The high-pressure cold spray system at *ASB Industries, Inc* was employed to spray metallic powders on the Mg alloy (a detailed procedure is given in Supporting Information (S1)). The characterization of the uncoated and coated AZ31B Mg alloy samples, before and after the immersion test, was carried out using scanning electron microscopy (SEM) and energy dispersive X-ray spectroscopy (EDS) attached to the SEM, optical microscopy (OM), X-ray diffraction (XRD) analysis, infinite focus 3D measurement (IFM) system, Vickers microhardness tester, and dry reciprocating sliding tests using Rtech-Tribometer at room temperature (detailed procedures in Supporting Information (S2)). The potentiodynamic polarization (PDP) tests were performed in a flat cell using VMP-300 Bio-logic potentiostat following a three-electrode setup (detailed procedure in Supporting Information (S2)). The immersion tests for bare, Ti and Ta/Ti coated Mg alloys were done in two sets. The first set of samples were immersed up to 48 h and EIS were done at 1 h, 2 h, 6 h, 12 h, 24 h, 36 h, and 48 h. The electrochemical impedance spectroscopy (EIS) was performed in the frequency range from 100 kHz to 10 mHz at open circuit potential (OCP). The second set of bare and coated samples were immersed for 168 h in HBSS (long term immersion test (bioactivity test)) and afterward rinsed with DI water followed by drying in air (the details are presented in Supporting Information (S2)).

## 3. Results and discussion

### 3.1. Characterization of the coatings

The morphology of the powder particles used in this research work is exhibited in supporting information (S3). The (CP)–Ti, and Ta powders both demonstrated a spherical morphology as shown in supporting information (S3). Fig. 1a and b demonstrate the surface morphology of as-sprayed Ti and Ta coatings, respectively. It is obvious that the high impact energies caused the severe plastic deformation in the coatings. The presence of more flattened particles with noticeable material jetting can be observed on Ta coating surface (Fig. 1b, its inset) in comparison with Ti coating (Fig. 1a and e). This difference could be correlated to the intense plastic deformation of Ta powder particles upon impact (Fig. 1b and f). The surface roughness average ($R_a$) of as-sprayed coatings was measured to be 1.89 μm and 2.23 μm for Ta (Fig. 1f) and Ti (Fig. 1e) coatings, respectively; whereas, $R_a$ for bare Mg alloy was 621.20 nm. Fig. 1g– l display the cross-sectional microstructure (by optical microscopy) of as-sprayed coatings on the AZ31B Mg alloys at different magnifications.

The as-sprayed Ta coating (with about 0.10% porosity level) displays a dense microstructure with no noticeable micro-pores (Fig. 1h and 1j) compared to Ti coatings (Fig. 1g and 1i). Severe plastic deformation of Ta powder particles upon impact can lead to a tight bonding at highly deformed inter-particle interface [32] and a substantial work hardening in the coating microstructure [18]. Furthermore, Ti coating (with about 0.50 ± 0.20% porosity level) represented slightly dense microstructure (Fig. 1g and 1i) with miniscule micro-pores and the local deformation of Ti powder is noticeable (Fig. 1k, and 1l). However, a higher level of porosities has been reported for the cold sprayed Ti coating (2.7%), warm sprayed Ti coatings (about 3.8–5.4%) and plasma sprayed Ti coating (10.2%) [17,27]. It looks that the Ta coating has considerably penetrated into the Ti layer with heavily deformation (Fig. 1h, j, and 1l). This could even lead to the densification of underneath sprayed layers (shot peening effect) via Ta particles with a high kinetic energy (Fig. 1l). Moreover, Ti particles profoundly infiltrated into the Mg alloy substrates (Fig. 1g, h and 1j). This behaviour is generally observed when hard particles, with a high kinetic energy impacted on the soft substrates [19]. Even though the coated AZ31B Mg alloys were sectioned, ground and polished before SEM and OM observations, the coating itself and coating/Mg alloy interface remained intact. No micro cracks and pores

are observed at layer/layer, and layer/substrate interfaces (Fig. 2a, e, 1g, 1h and 1j).

It is worth mentioning that high adhesion bond strength of the coating can be mainly ensured by strong mechanical interlocking (anchoring) between the coatings (within the coating) and Mg alloy substrate (Supporting Information (S4), showing Mg alloy and Ti layer extruded (extruded lips) in between Ti and Ta particles, respectively), [33,34]. The powder particles impact with high kinetic energy during high pressure cold spray (HPCS) process would lead to the stronger peening effect. In fact, the impacting powder particles may cause the intense deformation of the underneath sprayed layer during cold spray process [35]. This would be advantageous to the profounder infiltration of the sprayed powder particles into the Mg alloy substrate and also Ti intermediate layer in the Ta/Ti/Mg system. It was noticed that the deformation of the Mg alloy substrate and Ti layer (in the Ta/Ti coating) is about 58 μm (from the Ti coating/Mg alloy substrate interface) and 41 μm (from the Ta layer/Ti layer interface), respectively. This behavior was also observed by W. Sun et al. [36]. They reported that the bond strength of high-pressure cold-sprayed CoCrMo and Ti6Al4V coatings on 6061-T651 Al alloy is about 66.17 MPa and 50.38 MPa, respectively [36]. The higher shear bond strength of CoCrMo coating (with 2.51 ± 0.20% porosity level) compared to Ti6Al4V coating (with 2.83 ± 0.24% porosity level) was attributed to the higher density and hardness of the cold sprayed CoCrMo coating. The profounder infiltration of the sprayed powder particles into their substrate (or the underneath sprayed layer) is in line with the higher shear bonding strength results [36]. In this research, adherence between substrate and coatings (and also between layers) seems to be excellent with a no existence of either cracks or voids

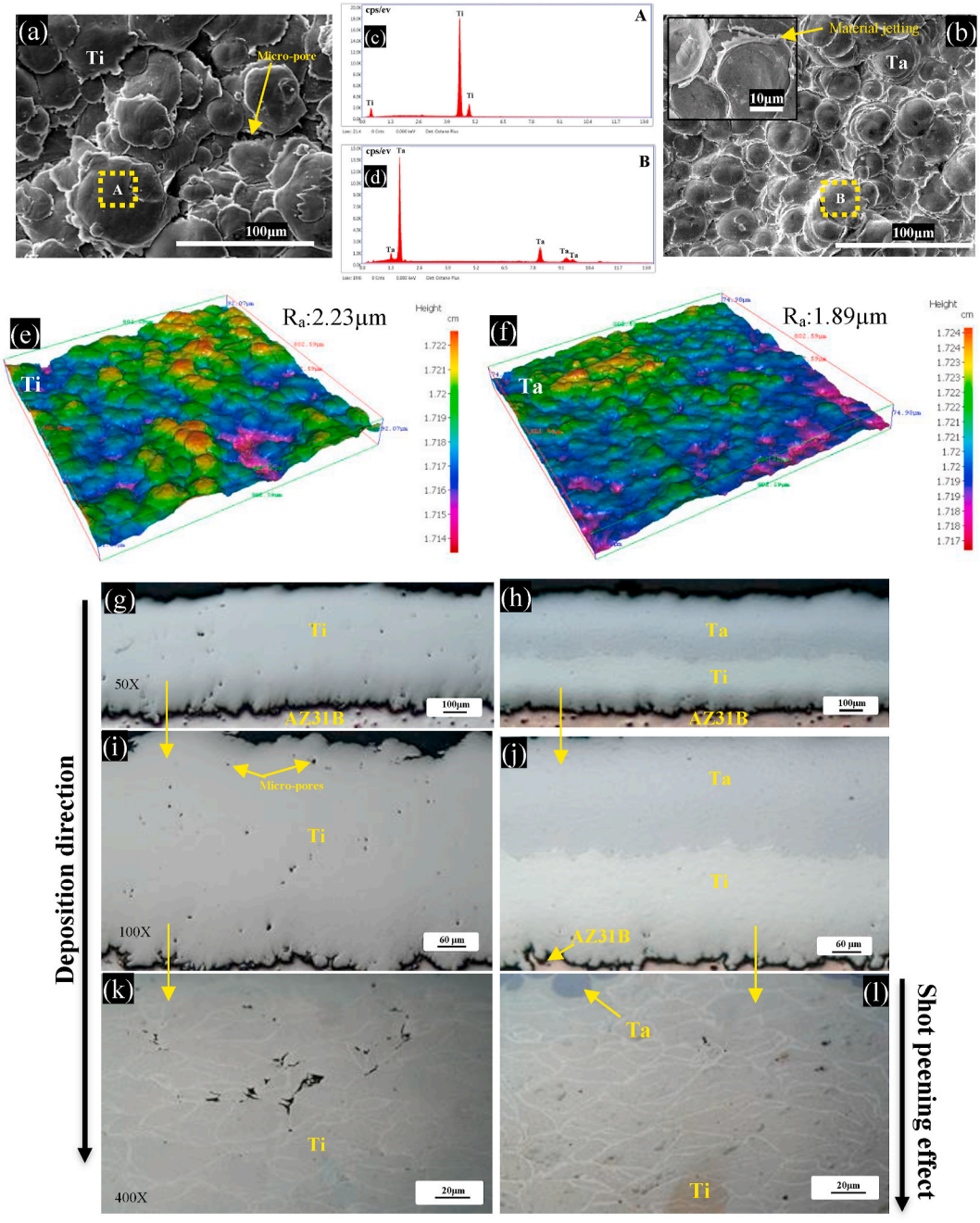


**Fig. 1.** Surface morphology of as-sprayed Ti (a) and Ta/Ti (b) coatings, (c) EDS area from a(A), (d) EDS area from b(B), surface topography of as-sprayed Ti(e) and Ta/Ti (f) coatings, cross-sectional microstructure of as-deposited Ti (g, i, k) and Ta/Ti (h, j, l) coatings on the AZ31B Mg alloys at different magnifications.

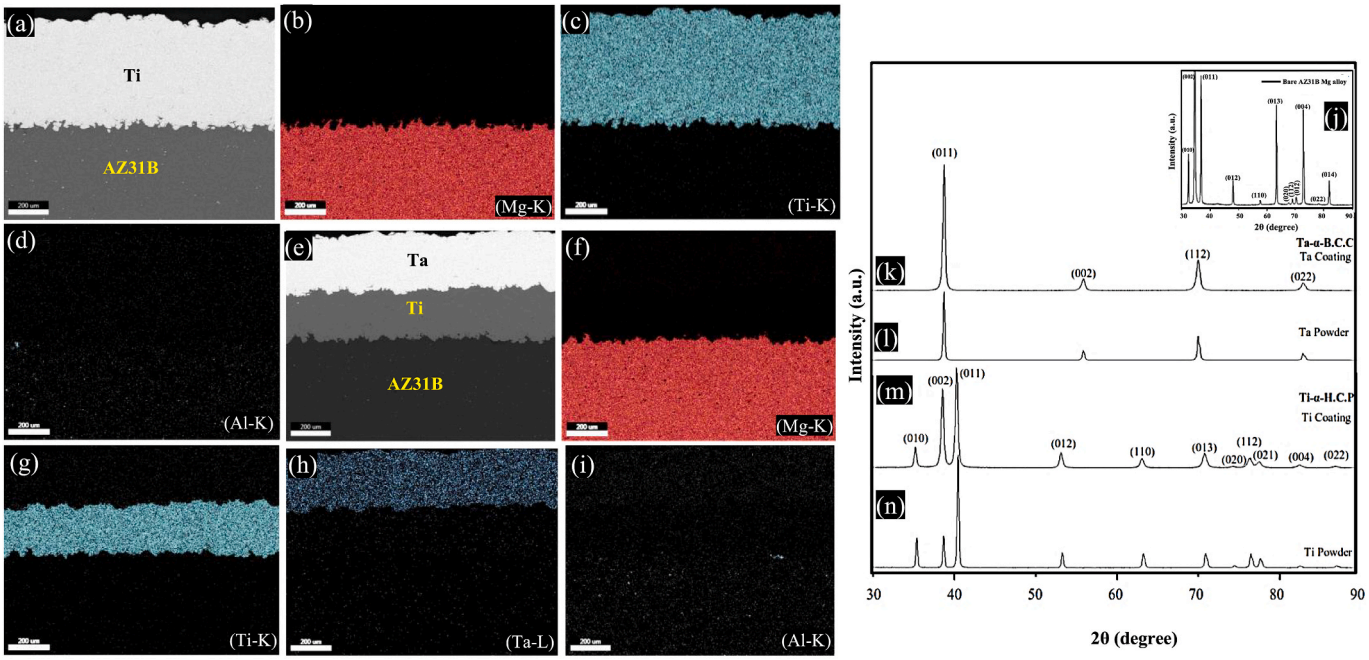


**Fig. 2.** (a–d) EDS map from polished cross section of Ti coated AZ31B Mg alloy, (e–i) EDS map from polished cross section of Ta/Ti coated AZ31B Mg alloy, (j–n) XRD patterns of AZ31B Mg alloy substrate, as-received powders and as-sprayed coatings.

at the interfaces, which is most likely attributed to the elevated powder particle velocities inherent to the high pressure cold spray process [18,19,37,38] and also the above-mentioned reasons.

Elemental analysis of surface and cross sectional of coated AZ31B Mg alloys were done using EDS spot analysis (Fig. 1c and d) and EDS maps (Fig. 2a–i), respectively. Mono-layered coating on AZ31B substrate is primarily comprised of Ti element (Figs. 1c and 2a-2d). Furthermore, bi-layered coating (Fig. 2e–i) on the substrate is constituted by Ti element (as first layer) and Ta element (as top sealant layer, Fig. 1d). XRD patterns of AZ31B Mg alloy substrate, as-received powders and as-sprayed coatings are depicted in Fig. 2j–n. AZ31B Mg alloy substrate is mostly constituted by α-Mg phase (H.C.P) (Fig. 2j). On the other hand, both powder and cold sprayed coating show the same phases and crystalline planes which are evidently discernible in (Fig. 2k–n). Any evidence of phase transformation and oxidation in the cold sprayed coatings cannot be observed (Fig. 2a–i and 2j-2n). The noticeable broadened peaks in XRD patterns of Ti (Fig. 2m) and Ta (Fig. 2k) coatings are principally correlated to the extreme plastic deformation of powder particles in the coatings during spraying process which has been observed by the previous investigators [36,39]. It is apparently seen that original phase and crystalline planes of powders were maintained in their coatings (Fig. 2k–n). This retention of phase and structure could be associated to the low temperature of spray process and substantial hammering effect of powder particles during cold spray process.

Ta coating ($HV_{0.025}$: 316.07) has greatly enhanced the hardness of Mg alloy ($HV_{0.025}$: 85.93) surface compared to Ti coating ($HV_{0.025}$: 257.67). A greater micro-hardness of Ta coating implies remarkable plastic deformation at inter-particle boundaries, which led to the enhancement of the coating compactness. Moreover, the surface coating with a highest hardness, i.e. Ta/Ti coating, provided a lowest wear rate followed by an increase for Ti coating and highest for bulk Mg (Supporting Information (S5)).

### 3.2. Electrochemical corrosion test results

Figs. 3–5 depict the electrochemical corrosion test results of coated and uncoated Mg alloys in SBF solution. Fig. 3a shows the OCP of samples versus elapsed time. OCP for uncoated, Ti coated and Ta/Ti coated Mg alloys was stabilized (at nobler potentials compared to the start of the immersion) at around −1549.80 mV to −152.2 mV, and −160 mV, respectively. The results show that Mg substrate with more active potential (lower OCP) is much more vulnerable to corrosion than coated samples with higher OCP. Dynamic equilibrium dissolution between the formations of oxide scale (film) on the electrode surface can results in the final steady OCP [33,40]. The potentiodynamic polarization curves for bare and coated AZ31B Mg alloy samples (after OCP stabilization for 60 min) in 3.5 wt% NaCl solution are displayed in Fig. 3b. In Ta/Ti coated Mg alloy, Ta top layer displays unstable passivation. It has been reported that a failure in the passive layer may lead to the formation of a pit [41]. However, the reparation in the passive layer at even higher potentials may take place when the pits are insignificant in size [41]. This behavior was also observed in the PDP curve of Ta/Ti coated Mg alloy and also reported by Heli Koivuluoto et al. and Balani et al. [32,42].

Ta top layer retained linear passivation (passive layer formation) at even higher potentials in comparison with the AZ31B alloy. It is postulated that severe plastic deformation of small Ta particles upon intense impact (Fig. 1b and f) could lead to the significant duplication of dislocations, induction of lattice micro-strain, refined crystals and residual stresses in the coating microstructure [43,44]. These could influence the unique corrosion behavior of the cold sprayed Ta layer.

Ti coated Mg alloy (anodic branch, Fig. 3b) depicts the typical passivation and pitting characteristics, which are slightly similar to the passivation behavior of bulk Ti in the SBF solution [45,46]. In fact, active dissolution of Mg alloy could substantially be lowered by the cold sprayed Ti coating (by two orders of magnitude), which displayed lower corrosion current density ($i_{corr}$, Table 3, Supporting Information (S1)) than bare AZ31B Mg alloy. E. Zhang et al. reported that $i_{corr}$ of pure Mg can be lowered by Ti coating (by only one order of magnitude) [2]. In the present work, Ta/Ti coated Mg alloy showed lower $i_{corr}$ (and average penetration corrosion rate, $C_R = 22.85 i_{corr}$ mm/year [47]) than Ti coated Mg alloy. Fig. 4a–d demonstrate the Nyquist and Bode plots of coated and uncoated Mg alloy samples. Electrical equivalent circuits (Fig. 4c: $X_1$ and $X_2$) were employed to fit the impedance spectra. The Nyquist plot of bare Mg alloy (per Fig. 4c (model $X_1$)) is comprised of one capacitive loop (at high frequency) and also one inductive loop (at

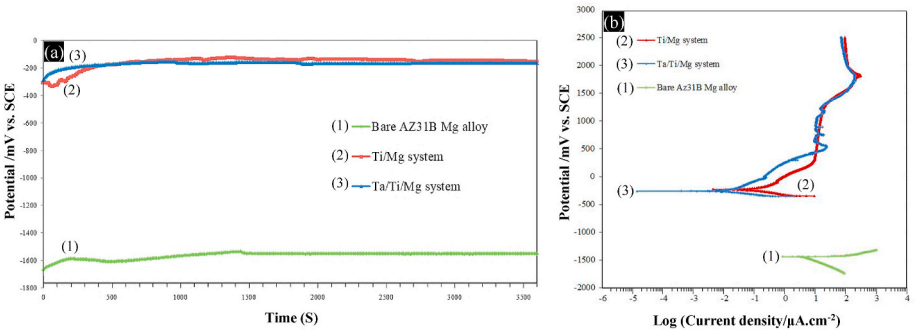


**Fig. 3.** Electrochemical corrosion test results of coated and uncoated Mg alloys in Hank's solution, (a) OCP for 1 h, (b) Potentiodynamic polarization (PDP) curves.

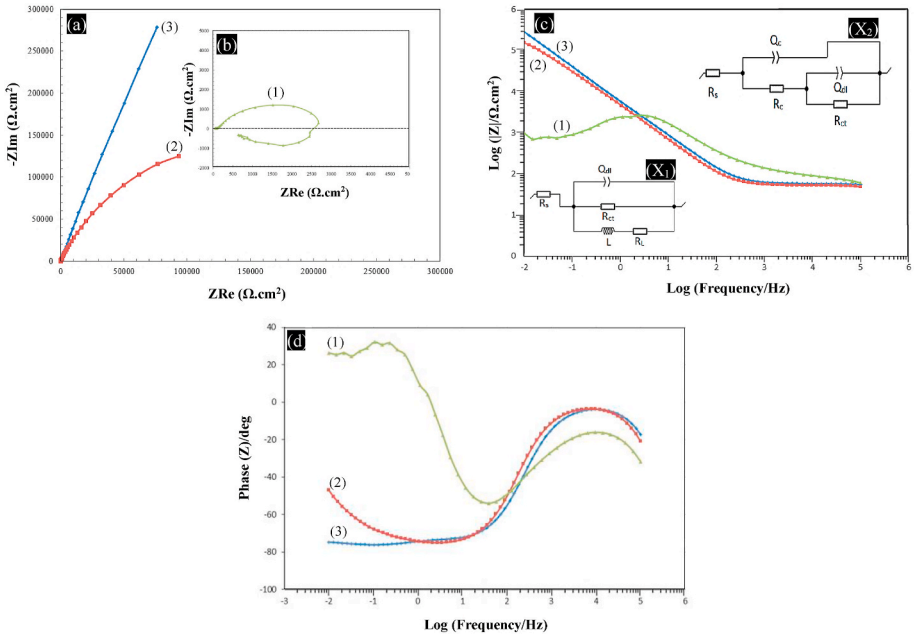


**Fig. 4.** Electrochemical corrosion test results of coated and uncoated Mg alloys in Hank's solution, (a, b) Nyquist plots at OCP, (c, d) Bode plots at OCP, ($X_1$, $X_2$): Electrical equivalent circuits (EEC) to fit the impedance spectra of bare and coated AZ31B Mg alloys, respectively; EEC elements including $R_{ct}$ (charge transfer resistance across the electric double layer at electrode/electrolyte interface), $R_s$ (solution resistance), $Q_{dl}$ (constant phase element for electric double layer), L (adsorption inductance), $R_L$ (adsorption resistance), $Q_c$ (constant phase element for surface film (outer)), $R_c$ (resistance that comprises the resistance of outer oxide film/corrosion products and resistance of the electrolyte in the pores); (1) bare AZ31B Mg alloy, (2) Ti/Mg, and (3) Ta/Ti/Mg systems.

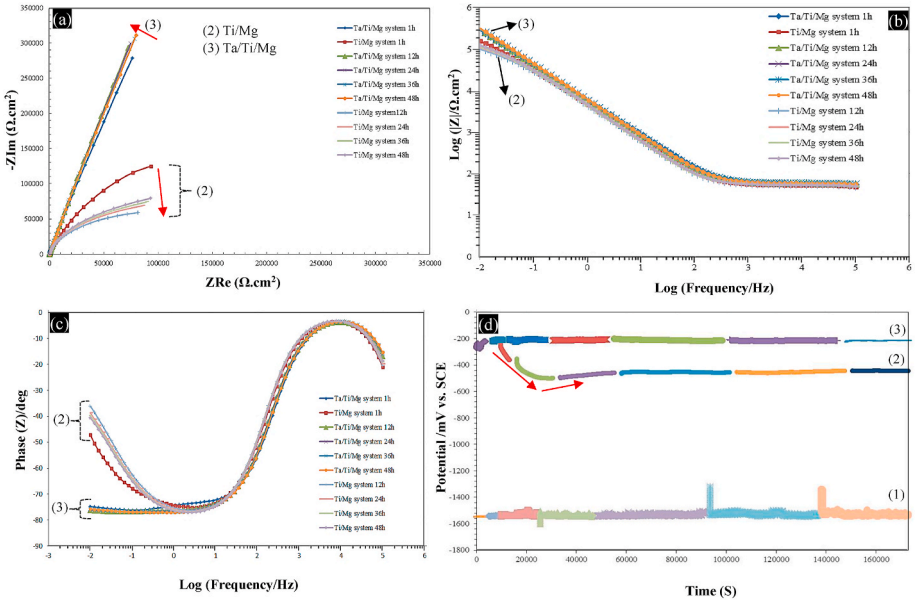


**Fig. 5.** (a–c) Nyquist and Bode plots of coated AZ31B Mg alloys during 48 h of immersion, and (d) OCP for 48 h; (1) bare AZ31B Mg alloy, (2) Ti/Mg, and (3) Ta/Ti/Mg systems.

low frequency). However, the two capacitive loops (at high and low frequency regions) were considered for the coated Mg alloys (Fig. 4c ($X_2$)).

The corrosion rate of the sample is inversely proportional to the $R_{ct}$ (charge transfer resistance across the inner electrical double layer at electrode/electrolyte interface) value [48]. The corrosion resistance for samples can be evaluated with absolute impedance ($|Z|_{f=0.01Hz}$) at a low frequency [48,49] (by bode magnitude plots (Fig. 4c)). Bare AZ31B Mg alloy revealed to have the highest corrosion rate among the three samples. This inference is pertained to the lesser $R_{ct}$ (2733 Ω $cm^2$) value for the bare AZ31B Mg alloy. This proves the low protection efficiency of corrosion surface layer (film) formed on the Mg alloys in chloride containing solutions. However, $R_{ct}$ values for Ti and Ta/Ti coated Mg alloys are 357.795 kΩ $cm^2$, and 24700 kΩ $cm^2$, respectively. This data indicates that Ti coating and particularly Ta/Ti coating can act as exceptional protective coatings on Mg alloys. Likewise, Ta/Ti coated Mg alloy showed the highest $|Z|_{f=0.01Hz}$ (or corrosion resistance [49,50]) among all samples (Fig. 4c). Bode phase plots (Fig. 4d) were noticeably enlarged and broadened (their aperture) after spraying metallic coatings on Mg substrates. This beneficial occurrence was related to the shielding capability of the coatings [48,51]. Ti and Ta/Ti coated AZ31B Mg alloy samples depicted maximum phase angle close to −75°(at relatively low-intermediate frequency) and −76° (at low-intermediate frequency), respectively.

It is evident that the $R_{ct}$ and $|Z|_{f=0.01Hz}$ values for Ta/Ti coated Mg alloy have remained slightly stable (Fig. 5a and b). Moreover, bode phase plots of Ta/Ti coated Mg alloy (Fig. 5c) showed same behavior during 48 h immersion. These impart that the rate of the electrochemical processes at the electrode/electrolyte interface could remain very slow in the course of immersion time. The OCP values for Ta/Ti coating have remained constant (with no obvious reduction in OCP) during the 48 h of immersion (Fig. 5d (3)). This behavior could originate from fairly dense structure of the Ta layer which can considerably impede the penetration of corrosive solution into the coating. In contrast, the OCP of Ti coating (Fig. 5d (2)) immediately lessened (approximately after 1 h of immersion). This could be attributed to the presence of micro-pores on the Ti surface (Fig. 1a), which can provide pathways for the electrolyte to infiltrate. However, constant increment of OCP (approximately after 6 h of immersion) could be ascribed to the reaction dynamic equilibrium between Ti element and the electrolyte [52], and corrosion product formation which may temporarily impede the further electrolyte infiltration into the inner regions of the Ti coating. These alterations were also seen in the Nyquist and Bode plots of Ti coated Mg alloys (Fig. 5a-c). Bare Mg alloy (Fig. 5d (1)) displayed the most negative potential compared to the coated Mg alloys, signifying that its tendency for corrosion is the highest. However, Ta/Ti coating presented the most

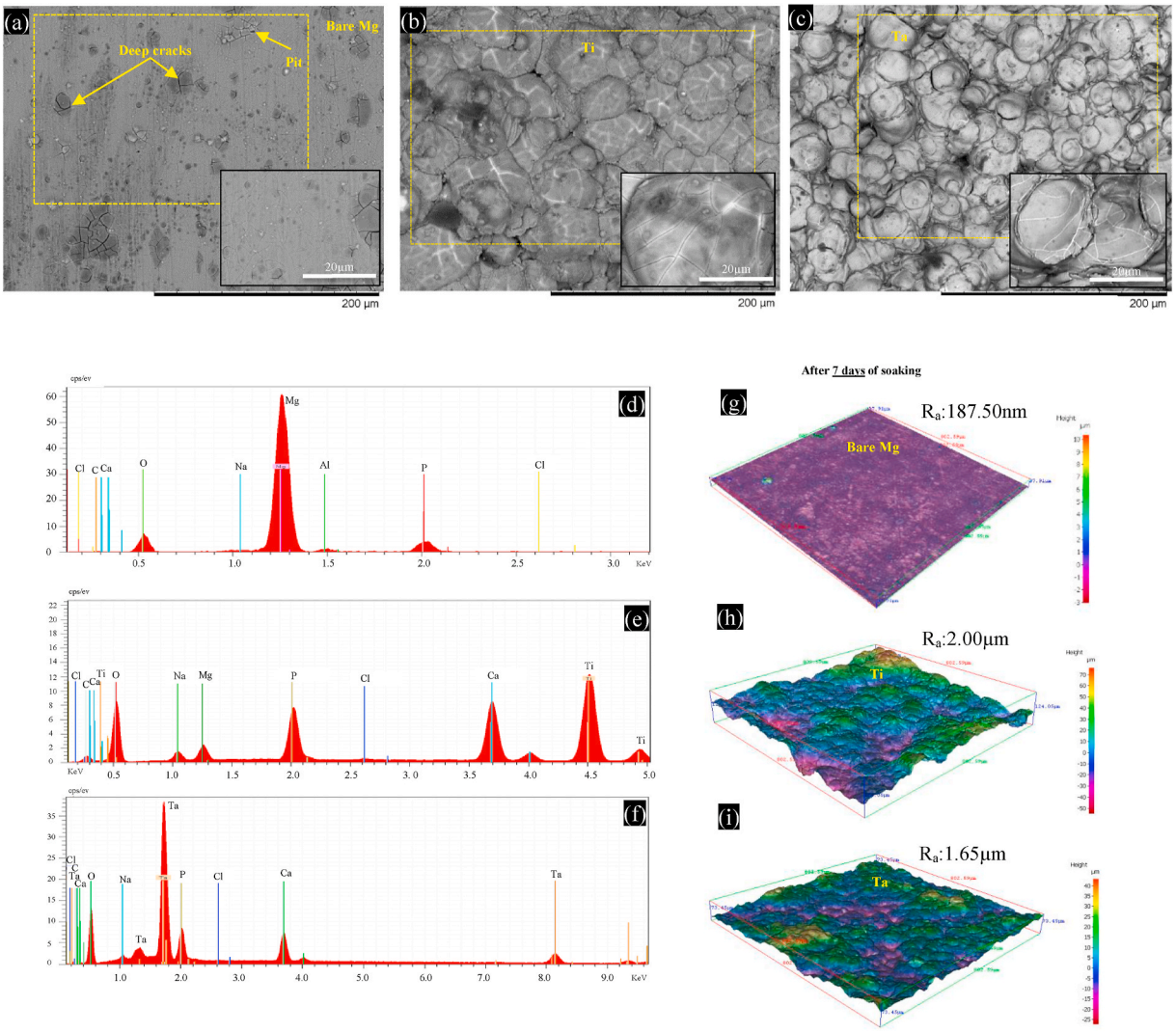


**Fig. 6.** Surface morphology of bare (a), Ti coated (b) and Ta/Ti coated (c) AZ31B Mg alloys, EDS analysis of uncoated (d), Ti coated (e) and Ta/Ti coated (f) samples surface, surface topography of bare (g), Ti coated (h) and Ta/Ti coated (i) AZ31B Mg alloys after long term immersion test (168 h in HBSS).

positive potential, highest $R_{ct}$, and highest$|Z|_{f=0.01Hz}$ values, suggesting that this coating is the least to be corroded (most thermodynamically stable) in Hank's solution over time.

### 3.3. Immersion test results in Hank's solution after 7 days

After 7 days of immersion, the water depletion of corrosion products and surface shrinkage led to the formation of (relatively deep and large) micro-cracks on AZ31B Mg alloy surface (Fig. 6a), followed by further penetration of the corrosive electrolyte [53]. Moreover, irregular corrosion products (apatite like compound containing Ca and P elements) covered a few regions of the Mg alloy surface (Figs. 6d and 7, and Supporting Information (S6)). In contrast, Ta top layer (consisting of highly protective oxide layer of Ta which remains stable at all pH range (Supporting Information (S7) [54])) successfully prevented the corrosive electrolyte penetration into the Ta/Ti/Mg system (Figs. 6f and 7 and Supporting Information (S8)). As depicted in Figs. 6f and 7, no Ti and Mg elements were detected on the Ta top layer surface. On the contrary, Mg element and Mg containing corrosion products were detected on the intact Ti coating (Supporting Information (S8)) surface (Figs. 6e and 7, and Supporting Information (S9)).

It is conspicuously seen that the nucleation and growth capability of Ca and P containing compounds on the surface of cold sprayed coatings (Fig. 6e and 6f) are greater than AZ31B Mg alloy surface (Fig. 6d) with the same exposure time in Hank's solution. In fact, Ca and P containing compounds enhance the surface bioactivity and strong fixation of an implant to the host bone can be enabled [55]. The Ca/P atomic ratio calculated from EDS results for AZ31B Mg alloy was about 0.79–1.01, while, the Ca/P ratio for the cold sprayed coatings was between 1.35 and 1.45; showing that more ions (carbonate and phosphate) can be absorbed by the cold sprayed coatings [15,53,56] after 7days of immersion in Hank's solution. This phenomenon suggested better bioactivity and osteoconductivity of the cold sprayed coatings compared to the bare AZ31B Mg alloy after 7days of immersion [53,57,and58]]. It was reported that the Ca/P atomic ratio of about 1.33 corresponds to Ca/P ratio of octacalcium phosphate (OCP) [58,59]. OCP is known to be an important precursor in the crystallization of bone-like apatite (hydroxyapatite) [60,61] and able to simulate the osteogenesis [58,61]. Better bioactivity and osteoconductivity of the cold sprayed coatings could be related to the highly passivating nature (Fig. 3b) [33,62,63] and the island-like rough surface of the cold sprayed Ti and Ta coatings (Fig. 6b, h and 6c, 6i) which are further conducive to the biological fixation [64,65], and can supply appropriate nucleation sites for the calcium-phosphate (Ca–P) compounds formation and growth in the SBF [66–69]. W. Jin et al., reported that a desirable surface for cell attachment, spreading, and proliferation can be achieved by applying a layer of Ta on the ZK60 Mg alloy. This was mainly attributed to the enhanced corrosion resistance of Mg alloy and considerable reduction of Mg activity which led to the substantial improvement of cytocompatibility of the ZK60 Mg alloy in SBF solution [70]. Although the present results from this research are pretty promising, in-vitro cell and even in-vivo experiments should be conducted to portray the decisive usefulness of Ta/Ti coated Mg alloys in the biomaterials field.

## 4. Conclusions

Ti and Ta/Ti coatings were applied on AZ31BMg alloy using high pressure cold spray process. These coatings with high hardness lowered the wear and corrosion rates of the Mg alloy. A part of Ti coating thickness was replaced by a dense layer of Ta which markedly lowered the corrosion rate (considerable increment of $R_{ct}$) of Ti coated Mg alloy in the Hank's balanced salt solution. Moreover, better bioactivity was

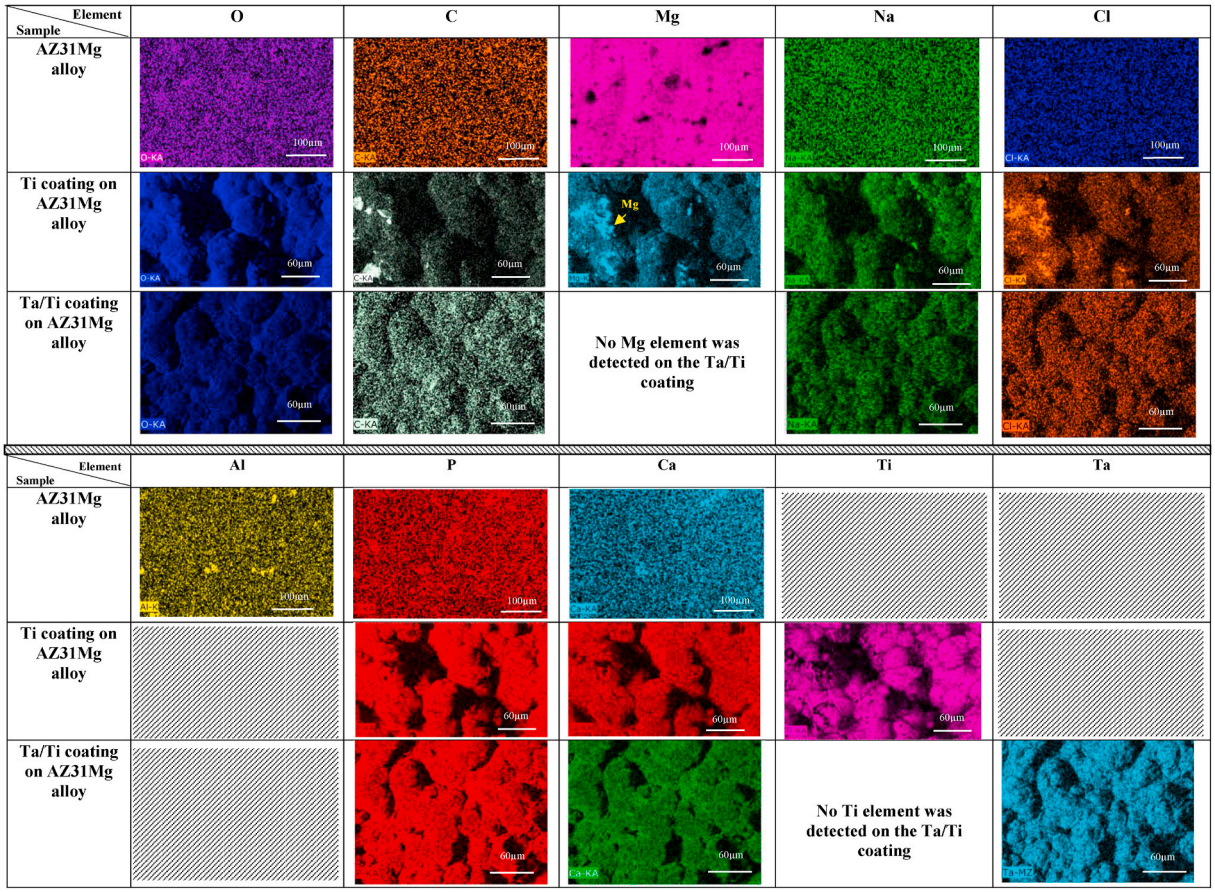


**Fig. 7.** EDS maps from surface of bare and coated AZ31B Mg alloys after long term immersion test (168 h in HBSS).

noticeably observed on the Ti and Ta/Ti coatings surface compared to bare AZ31B Mg alloy surface. This behaviour was attributed to highly passivating nature of the cold sprayed Ti and Ta/Ti coatings and also the rough surface (island-like) of these coatings which can supply appropriate nucleation sites for the formation and growth of calcium-phosphate (Ca–P) compounds in Hank's balanced salt solution.

The OCP values for Ta/Ti coating remained constant (with no obvious reduction in OCP) during the 48 h of immersion. This behavior originated from fairly dense structure of the Ta layer which considerably impeded the penetration of corrosive solution into the coating. Ta/Ti coating presented the most positive potential, highest $R_{ct}$ (charge transfer resistance), and highest$|Z|_{f=0.01Hz}$ values, suggesting that it is the most thermodynamically stable/least to be corroded in Hank's balanced salt solution over time. Likewise, Ta top layer successfully prevented the corrosive electrolyte penetration into the Ta/Ti/Mg system. As, no Ti and Mg elements were detected on the Ta top layer surface after 7 days of immersion. The results show that Ta/Ti coating not only improves the bioactivity of AZ31BMg alloy but also substantially enhances the corrosion resistance of bare and Ti coated AZ31B Mg alloy in Hank's balanced salt solution.

## CRediT authorship contribution statement

**M. Daroonparvar:** Conceptualization, Data curation, Formal analysis, Investigation, Methodology, Validation, Visualization, Writing - original draft, Supervision, Project administration, Writing - review & editing. **M.U. Farooq Khan:** Methodology, Validation, Visualization, Writing - review & editing. **Y. Saadeh:** Methodology, Validation, Visualization, Writing - review & editing. **C.M. Kay:** Funding acquisition, Resources, Writing - review & editing. **R.K. Gupta:** Funding acquisition, Resources, Investigation, Validation, Visualization, Project administration, (corrosion tests and characterizations after corrosion tests), Writing - review & editing. **A.K. Kasar:** Methodology, Validation, Visualization, Writing - review & editing. **P. Kumar:** Methodology, Validation, Visualization, Writing - original draft, Writing - review & editing. **M. Misra:** Funding acquisition, Resources, Project administration, (characterization section), Writing - review & editing. **P. Menezes:** Project administration, (wear tests), Writing - review & editing. **H.R. Bakhsheshi-Rad:** Writing - review & editing.

## Declaration of competing interest

The authors declare that they have no known competing financial interests or personal relationships that could have appeared to influence the work reported in this paper.

## Acknowledgements

The authors would like to acknowledge the ASB Industries, Inc for providing facilities and financial support. R. K. Gupta acknowledges the financial support from the National Science Foundation (NSF-CMMI 1846887) under the direction of Dr. Alexis Lewis. M. Misra duly acknowledges the startup fund from the University of Nevada: Reno.

## Appendix A. Supplementary data

Supplementary data to this article can be found online at https://doi.org/10.1016/j.matchemphys.2020.123627.

## References

[1] X. Liu, et al., Binary Titanium Alloys as Dental Implant Materials—A Review, Regenerative Biomaterials, 2017, pp. 315–323.
[2] E. Zhang, L. Xu, K. Yang, Formation by ion plating of Ti-coating on pure Mg for biomedical applications, Scripta Mater. 53 (2005) 523–527.
[3] R. Radha, D. Sreekanth, Insight of magnesium alloys and composites for orthopedic implant applications–a review, Journal of Magnesium and Alloys 5 (2017) 286–312.
[4] Y. Yang, et al., Mg bone implant: features, developments and perspectives, Mater. Des. 185 (2020) 108259.
[5] C. Shuai, et al., 3D honeycomb nanostructure-encapsulated magnesium alloys with superior corrosion resistance and mechanical properties, Composites Part B 162 (2019) 611–620.
[6] H.R. Bakhsheshi-Rad, et al., Coating biodegradable magnesium alloys with electrospun poly-L-lactic acid-åkermanite-doxycycline nanofibers for enhanced biocompatibility, antibacterial activity, and corrosion resistance, Surf. Coating. Technol. 377 (2019) 124898.
[7] Y. Wu, et al., Hydrothermal fabrication of rGO/Apatite layers on AZ31 magnesium alloy for enhanced bonding strength and corrosion resistance, Appl. Surf. Sci. 470 (2019) 430–438.
[8] C. Shuai, et al., Interfacial strengthening by reduced graphene oxide coated with MgO in biodegradable Mg composites, Mater. Des. 191 (2020) 108612.
[9] L.B. Tong, et al., Enhanced corrosion and wear resistances by graphene oxide coating on the surface of Mg-Zn-Ca alloy, Carbon 109 (2016) 340–351.
[10] C. Shuai, et al., Biodegradable metallic bone implants, Materials Chemistry frontiers 3 (2019) 544–562.
[11] J. Gray, B. Luan, Protective coatings on magnesium and its alloys—a critical review, Alloys and Compounds 336 (1–2) (2002) 88–113.
[12] S. Singh, et al., Corrosion behavior and characterization of HA/$Fe_3O_4$/CS composite coatings on AZ91 Mg alloy by electrophoretic deposition, Mater. Chem. Phys. 237 (2019) 121884.
[13] B. Singh, et al., In-vitro assessment of HA-Nb coating on Mg alloy ZK60 for biomedical applications, Mater. Chem. Phys. 231 (2019) 138–149.
[14] S. Kumar, et al., Imparting increased corrosion passive and bio-active character to $Al_2O_3$ based ceramic coating on AZ91 alloy, Surf. Coating. Technol. 383 (2020) 125231.
[15] H.L. Yao, et al., Improved corrosion resistance of AZ91D magnesium alloy coated by novel cold-sprayed Zn-HA/Zn double-layer coatings, Ceram. Int. 6 (2020) 7687–7693.
[16] D. Zhang, et al., A comparative study on the corrosion behavior of Al, Ti, Zr and Hf metallic coatings deposited on AZ91D magnesium alloys, Surf. Coating. Technol. 303 (2016) 94–102.
[17] B. Moronczyk, E. Ura-Binczyk, S. Kuroda, J. Jaroszewicz, R.M. Molak, Microstructure and corrosion resistance of warm sprayed titanium coatings with polymer sealing for corrosion protection of AZ91E magnesium alloy, Surf. Coating. Technol. 363 (2019) 142–151.
[18] Z. Monette, A. K Kasar, M. Daroonparvar, P. L Menezes, Supersonic particle deposition as an additive technology: methods, challenges, and applications, Int. J. Adv. Manuf. Technol. 106 (2020) 2079–2099.
[19] C.M. Kay, J. Karthikeyan, High Pressure Cold Spray: Principles and Applications, ASM International, 2016, ISBN 978-1-62708-096-5.
[20] M. Daroonparvar, M.A. M Yajid, N.M. Yusof, H.R. Bakhsheshi-Rad, Fabrication and properties of triplex NiCrAlY/nano Al2O3· 13% TiO2/nano TiO2 coatings on a magnesium alloy by atmospheric plasma spraying method, Alloys and Compounds 645 (2015) 450–466.
[21] X.T. Luo, et al., High velocity impact induced microstructure evolution during deposition of cold spray coatings: a review, Surf. Coating. Technol. 254 (2014) 11–20.
[22] H. Asadi, et al., Cold spraying: a materials perspective, Acta Mater. 116 (2016) 382–407.
[23] M. Daroonparvar, M.A. Mat Yajid, N.M. Yusof, H.R. Bakhsheshi-Rad, E. Hamzah, Microstructural characterisation of air plasma sprayed nanostructure ceramic coatings on Mg–1% Ca alloys (bonded by NiCoCrAlYTa alloy), Ceram. Int. 42 (2016) 357–371.
[24] J. Wang, X. Pang, and H. Jahed, Surface protection of Mg alloys in automotive applications: a review, AIMS Materials Science, 6(4): 567–600..
[25] X. Zhou, P. Mohanty, Corrosion behaviour of cold sprayed titanium coatings in simulated body fluid, Corrosion Eng. Sci. Technol. 47 (2012) 145–154.
[26] W. Yang, et al., Microstructure and properties of duplex coatings on magnesium alloy, Surf. Eng. 32 (2016) 601–606.
[27] J. Cizek, et al., Influence of plasma and cold spray deposited Ti Layers on high-cycle fatigue properties of Ti6Al4V substrates, Surf. Coating. Technol. 217 (2013) 23–33.
[28] F. Khodabakhshi, et al., Surface modification of a cold gas dynamic spray-deposited titanium coating on aluminum alloy by using friction-stir processing, J. Therm. Spray Technol. 28 (2019) 1158–1198.
[29] V. Balla, et al., Direct laser processing of a tantalum coating on titanium for bone replacement structures, Acta Biomater. 6 (2010) 2329–2334.
[30] A. Ching Hee, et al., Corrosion behaviour and adhesion properties of sputtered tantalum coating on Ti6Al4V substrate, Surf. Coating. Technol. 307 (2016) 666–675.
[31] A. Ching Hee, et al., Tribo-corrosion performance of filtered-arc-deposited tantalum coatings on Ti-13Nb-13Zr alloy for bio-implants applications, Wear 400–401 (2018) 31–42.
[32] H. Koivuluoto, et al., Corrosion resistance of cold-sprayed Ta coatings in very aggressive conditions, Surf. Coating. Technol. 205 (2010) 1103–1107.
[33] Y.K. Wei, Y. Juan Li, Y. Zhang, X. Tao Luo, C. Jiu Li, Corrosion resistant nickel coating with strong adhesion on AZ31B magnesium alloy prepared by an in-situ shot-peening-assisted cold spray, Corrosion Sci. 138 (2018) 105–115.

[34] A.W.Y. Tan, et al., Influence of particle velocity when propelled using $N_2$ or $N_2$-He mixed gas on the properties of cold-sprayed Ti6Al4V coatings, coatings, Coatings 8 (2018) 1–22, 327.
[35] S. Siddique, et al., Enhanced electrochemical and tribological properties of AZ91D magnesium alloy via cold spraying of aluminum alloy, J. Therm. Spray Technol. (2019) 20.
[36] W. Sun, et al., Adhesion, tribological and corrosion properties of cold-sprayed CoCrMo and Ti6Al4V coatings on 6061-T651 Al alloy, Surf. Coating. Technol. 326 (2017) 291–298.
[37] J. Chen, et al., Wear and corrosion properties of 316L-SiC composite coating deposited by cold spray on magnesium alloy, J. Therm. Spray Technol. 26 (2017) 1381–1392.
[38] V. Champagne, The Cold Spray Materials Deposition Process, Fundamentals and Applications: *The Advantages and Disadvantages of the Cold Spray Coating Process Chapter*, first ed., Woodhead Publishing, 2007, ISBN 9781845693787.
[39] W. Sun, , et al.E. Liu, Effect of substrate surface condition on fatigue behavior of cold sprayed Ti6Al4V coatings, Surf. Coating. Technol. 320 (2017) 452–457.
[40] T. Marocco, et al., Corrosion performance of laser post treated cold sprayed titanium coatings, J. Therm. Spray Technol. 20 (2011) 909–917.
[41] P.A. Schweitzer (Ed.), Corrosion Engineering Handbook, Marcel Dekker, 1996, p. 736.
[42] K. Balani, et al., Effect of carrier gases on microstructural and electrochemical behavior of cold-sprayed 1100 aluminum coating, Surf. Coating. Technol. 195 (2005) 272–279.
[43] Z. Arabgol, et al., Analysis of thermal history and residual stress in cold sprayed coatings, J. Therm. Spray Technol. 23 (2014) 84–90.
[44] H. Koivuluoto, et al., Cold sprayed copper and tantalum coatings: detailed FESEM and TEM analysis, Surf. Coating. Technol. 204 (2010) 2353–2361.
[45] X. Zhou, et al., Electrochemical behavior of cold sprayed hydroxyapatite/titanium composite in Hanks' solution, Electrochim. Acta 65 (2012) 134–140.
[46] I. da Silva Vieira Marques, et al., Electrochemical behavior of bioactive coatings on cp-Ti surface for dental application, Corrosion Sci. 100 (2015) 133–146.
[47] Z. Shi, et al., Measurement of the corrosion rate of magnesium alloys using Tafel extrapolation, Corrosion Sci. 52 (2010) 579–588.
[48] R. Maurya, et al., An environment-friendly phosphate chemical conversion coating on novel Mg-9Li-7Al-1Sn and Mg-9Li-5Al-3Sn-1Zn alloys with remarkable corrosion protection, Appl. Surf. Sci. 443 (2018) 429–440.
[49] Z. Lia, Effect of phosphate additive on the morphology and anti-corrosion performance of plasma electrolytic oxidation coatings on magnesium–lithium alloy, Corrosion Sci. 157 (2019) 295–304.
[50] X. Liu, et al., A combined coating strategy based on atomic layer deposition for enhancement of corrosion resistance of AZ31 magnesium alloy, Appl. Surf. Sci. 434 (2018) 1101–1111.
[51] M. Daroonparvar, et al., Deposition of duplex MAO layer/nanostructured titanium dioxide composite coatings on Mg–1% Ca alloy using a combined technique of air plasma spraying and micro arc oxidation, Alloys and Compounds 649 (2015) 591–605.
[52] C. Xie, et al., Corrosion behavior of cold sprayed pure zinc coating on magnesium, Surface & coatings technology, Surf. Coating. Technol. 374 (2019) 797–806.
[53] H.R. Bakhsheshi-Rad, et al., In vitro degradation behavior, antibacterial activity and cytotoxicity of $TiO_2$-MAO/ZnHA composite coating on Mg alloy for orthopedic implants, Surf. Coating. Technol. 334 (2018) 450–460.
[54] E. McCafferty, Thermodynamics of Corrosion: Pourbaix Diagrams, Introduction to Corrosion Science, Springer, 2009, pp. 95–117.
[55] M. Mohedano, et al., Bioactive plasma electrolytic oxidation coatings on Mg-Ca alloy to control degradation behavior, Surf. Coating. Technol. 315 (2017) 454–467.
[56] H.R. Bakhsheshi-Rad, et al., Fabrication and corrosion behavior of Si/HA nano-composite coatings on biodegradable Mg–Zn–Mn–Ca alloy, Surf. Coating. Technol. 258 (2014) 1090–1099.
[57] M. Yousefpour, et al., Bioactive layer formation on alkaline-acid treated titanium in simulated body fluid, Mater. Des. 28 (2007) 2154–2159.
[58] S.M. Choi, et al., Effect of surface modification on the in vitro calcium phosphate growth on the surface of poly (methyl methacrylate) and bioactivity, Colloids Surf. B Biointerfaces 76 (2010) 326–333.
[59] Y. Jang, et al., Effect of biologically relevant ions on the corrosion products formed on alloy AZ31B: an improved understanding of magnesium corrosion, Acta Biomater. 9 (2013) 8761–8770.
[60] A. Roguska, et al., Characterization of a calcium phosphate–$TiO_2$ nanotube composite layer for biomedical applications, Mater. Sci. Eng. C 31 (2011) 906–914.
[61] O. Suzuki, Octacalcium phosphate: osteoconductivity and crystal chemistry, Acta Biomater. 6 (2010) 3379–3387.
[62] H. Cao, et al., Activating titanium oxide coatings for orthopedic implants, Surf. Coating. Technol. 233 (2013) 57–64.
[63] V.K. Balla, et al., Direct laser processing of a tantalum coating on titanium for bone replacement structures, Acta Biomater. 6 (2010) 2329–2334.
[64] V. AM, et al., Osteoblastic cell response on high-rough titanium coatings by cold spray, J. Mater. Sci. Mater. Med. 29 (2018) 19.
[65] M. Heiden, S. Huang, E. Nauman, D. Johnson, L. Stanciu, Nanoporous metals for biodegradable implants: initial bone mesenchymal stem cell adhesion and degradation behavior, J. Biomed. Mater. Res. 7 (2016) 1747–1758.
[66] S. Cengiz, A. Uzunoglu, L. Stanciu, et al., Direct fabrication of crystalline hydroxyapatite coating on zirconium by single-step plasma electrolytic oxidation process, Surf. Coating. Technol. 301 (2016) 74–79.
[67] W. Jin, et al., Corrosion resistance and cytocompatibility of tantalum-surface-functionalized biomedical ZK60 Mg alloy, Corrosion Sci. 114 (2017) 45–56.
[68] M. Daroonparvar, M. Azizi Mat Yajid, Rajeev Kumar Gupta, Noordin Mohd Yusof, Hamid Reza Bakhsheshi Rad, Hamidreza Ghandvar, Ehsan Ghasemi, Antibacterial activities and corrosion behavior of novel PEO/nanostructured $ZrO_2$ coating on Mg alloy, Trans. Nonferr. Metal. SOC. 28 (8) (August 2018) 1571–1581.
[69] H.R. Bakhsheshi-Rad, E. Hamzah, M. Kasiri Asgarani, S. Jabbarzare, M. Daroonparvar, A. Najafinezh, Fabrication, degradation behavior and cytotoxicity of nanostructured hardystonite and titania/hardystonite coatings on Mg alloys, Vacuum 129 (July 2016) 9–12.
[70] Mohammadreza Daroonparvar, Muhamad Azizi Mat Yajid, Hamid Reza Bakhsheshi-Rad, Rajeev Kumar Gupta, A.F. Ismail, Study of corrosion behavior and In vitro bioactivity of single $NbSi_2$ and duplex $NbSi_2/Nb_5Si_3$ coatings on Nb substrates for biomedical applications, Prot. Met. Phys. Chem. Surf. 56 (2020) 628–637.